Supporting Information

Facile Synthesis of Flower-like Morphology of $Cu_{0.27}Co_{2.73}O_4$ for High-Performance Supercapacitor with Extraordinary Cycle Stability

Shipra Raj,[1] Pradip Kar,[1] Poulomi Roy[2]*

[1]Department of Chemistry, Birla Institute of Technology, Mesra, Ranchi 835215, Jharkhand, India

[2]Materials Processing & Microsystems Laboratory, CSIR - Central Mechanical Engineering Research Institute (CMERI), Mahatma Gandhi Avenue, Durgapur 713209, West Bengal, University, India

Email: *poulomiroy@yahoo.com; p.roy@cmeri.res.in*

Experimental details

Materials synthesis

All the chemicals used in our experiments were of analytical grade and were used without further purification. In a typical procedure, 40 mM of copper(II) nitrate trihydrate (Merck, 99.5%) and 80 mM cobalt(II) acetate tetrahydrate (Sigma-Aldrich, 98.0%) were mixed together in 15 mL deion-ized water followed by the addition of ammonia solution (25%) in excess under stirring and maintenance of a pH value of 12. The Ni-foam was treated with 6 M HCl under sonication for 30 min to remove the native oxide layer, and cleaned with acetone, ethanol and distilled water. The pre-treated Ni-foam was then placed into a beaker and kept in an oven at 90 °C for the slow evaporation of ammonia. After 20 h, the Ni-foam was collected, and cooled down to room temperature naturally. The sample was then sonicated in distilled water for 1 min to remove loosely adhered particles and dried in an oven at 50 °C. The as deposited precursor material was then calcined at 350 °C for 2 h in air to obtain $Cu_{0.27}Co_{2.73}O_4$ on Ni-foam. The deposition of Co_3O_4 nanoflakes and CuO nanostructure on Ni foam were carried out in similar way using 40 mM of respective metal precursors.

Under ammonia evaporation technique, the formation of $Cu_{0.27}Co_{2.73}O_4$ involved following chemical reactions:

$Co^{2+} + 6NH_3 \rightarrow [Co(NH_3)_6]^{2+}$ ...(S-1)

$Cu^{2+} + 4NH_3 + 2H_2O \rightarrow [Cu(NH_3)_4(H_2O)_2]^{2+}$ ...(S-2)

$[Co(NH_3)_6]^{2+} + [Cu(NH_3)_4(H_2O)_2]^{2+} + OH^- \rightarrow$ CuCo-hydroxide $\rightarrow Cu_{0.27}Co_{2.73}O_4$ ...(S-3)

The formation of Co3O4 and CuO occur according to the following chemical reactions:

$Co^{2+} + 6NH_3 \rightarrow [Co(NH_3)_6]^{2+}$ …(S-4)

$[Co(NH_3)_6]^{2+} + OH^- \rightarrow$ Co-hydroxide $\rightarrow Co_3O_4$ …(S-5)

$Cu^{2+} + 4NH_3 + 2H_2O \rightarrow [Cu(NH_3)_4(H_2O)_2]^{2+}$ …(S-6)

$[Cu(NH_3)_4(H_2O)_2]^{2+} + OH^- \rightarrow$ Cu-hydroxide $\rightarrow$ CuO …(S-7)

Characterization

X-ray diffraction (XRD) patterns of the materials were recorded on a Philips PW-1710 X-ray diffractometer (40 kV, 20 mA) using Cu Ka radiation (λ = 1.5418 Å) in the 2θ range of 10–70º. X-ray photoelectron spectroscopy (XPS) was performed on a PHI 5000 Versa Probe II (ULVAC-PHI, INC, Japan) system using a micro- focused (100 mm, 25 W, 15 kV) monochromatic Al Ka source (hν = 1486.6 eV), a hemispherical analyzer, and a multichannel detector. The typical vacuum in the analysis chamber during the measurements was in the range of 1×10^{-10} Torr. Charge neutralization was used for all measurements using a combination of low energy Ar^+ ions and electrons. The binding energy scale was charge referenced to the C 1s at 284.6 eV. The morphology of the samples was characterized by field-emission scanning electron microscopy (FE-SEM, Sigma HD, Carl Zeiss, Germany) and the compositions of the samples were determined by energy-dispersive X- ray analysis (EDX). The microstructures of samples were examined by High-Resolution Transmission Electron Microscopy (HR-TEM) on TECNAI G2, SEI (Netherland) operating at 200 kV. Prior to the analysis, the samples were prepared by drop casting on carbon-coated copper grids and drying overnight under vacuum.

Electrochemical measurement

The electrochemical measurements were performed in an AUTOLAB electrochemical workstation (AUTOLAB 302N) using 1 M KOH as electrolyte. In a three-electrode configuration, the binder-free sample deposited on Ni-foam itself was used as the working electrode, Pt as the counter electrode and Ag/AgCl as the reference electrode. In two-electrode cell configuration (asymmetric device), the as-prepared samples and activated carbon (AC) electrodes were used as the positive and negative electrodes, respectively.

The possible electrochemical reactions are as follows:

$Cu_{0.27}Co_{2.73}O_4 + H_2O + e^- \leftrightarrow CoOOH + CuOH$ …(S-8)

$CoOOH + OH^- \leftrightarrow CoO_2 + H_2O + e^-$ …(S-9)

$CuOH + OH^- \leftrightarrow Cu(OH)_2 + e^-$ …(S-10)

The specific capacity (C_s) in terms of C g^{-1} and specific capacitance (C_s') in F g^{-1} (to compare with literature) have been calculated as per the equation (S1) and (S2).

$$C_s = \frac{I \times \Delta t}{m} \text{ in C g}^{-1} \quad \text{...(S-11)}$$

$$C_s^{'} = \frac{I \times \Delta t}{m \times \Delta V} \text{ in F g}^{-1} \quad \text{...(S-12)}$$

where, I is the discharge current, Δt is the discharge time, m is the mass of the active material, and ΔV is the potential window.

In order to maintain the charge balance in the device, the mass loading of activated carbon was manipulated following the mass ratio as given below:

$$Q_+ = Q_- \quad \text{...(S-13)}$$

$$C_+ \times m_+ \times \Delta V_+ = C_- \times m_- \times \Delta V_- \quad \text{...(S-14)}$$

$$\frac{m_+}{m_-} = \frac{C_- \times \Delta V_-}{C_+ \times \Delta V_-} \quad \text{...(S-15)}$$

According to the charge balance theory, while CCO//AC device was fabricated with optimal mass ratio $\frac{m_+}{m_-}$ of 0.11, for CO//AC and CuO//AC devices obtained mass ratios were 0.2 and 0.33, respectively.[1, 2]

The energy density and power density of asymmetric devices were determined using the following equations:

$$E = \frac{1}{7.2} C (\Delta V)^2 \quad \text{...(S-16)}$$

$$P = 3600 \frac{E}{\Delta t} \quad \text{...(S-17)}$$

where, E is the energy density (Wh kg^{-1}), P represents the power density (W kg^{-1}), C refers to the specific capacitance (F g^{-1}), ΔV is the potential window (V), and Δt is the discharge time (s).

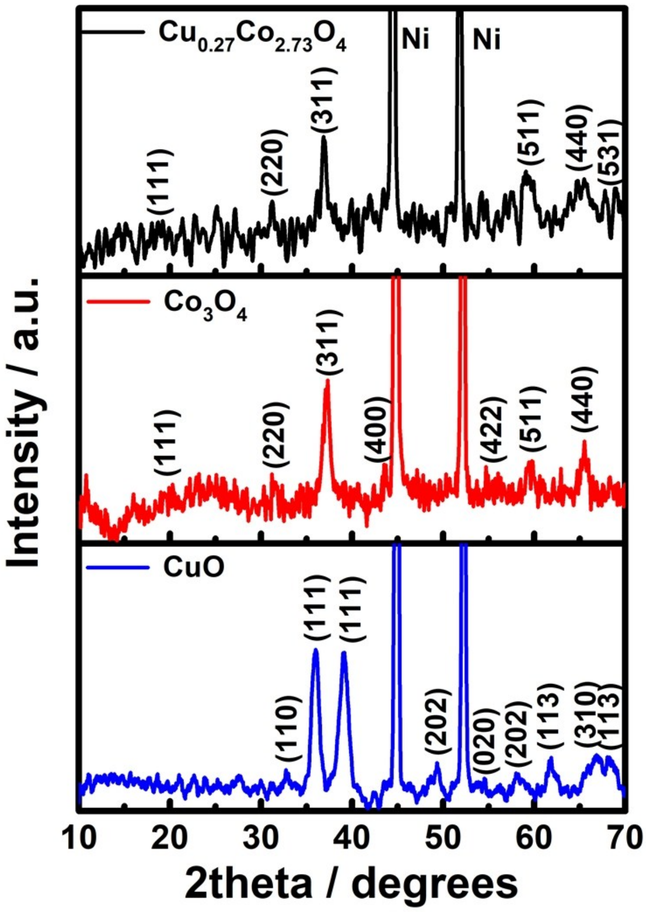

Figure S1: XRD patterns of $Cu_{0.27}Co_{2.73}O_4$ (JCPDS No. 78-2173), Co_3O_4 (JCPDS No. 76-1802) and CuO (JCPDS No. 80-0076) deposited on Ni foam.

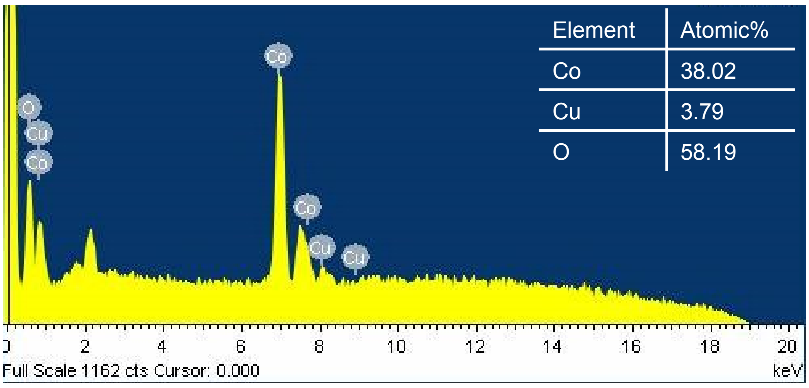

Element	Atomic%
Co	38.02
Cu	3.79
O	58.19

Figure S2: EDX analysis of $Cu_{0.27}Co_{2.73}O_4$ indicating the presence of Co as well as Cu along with O.

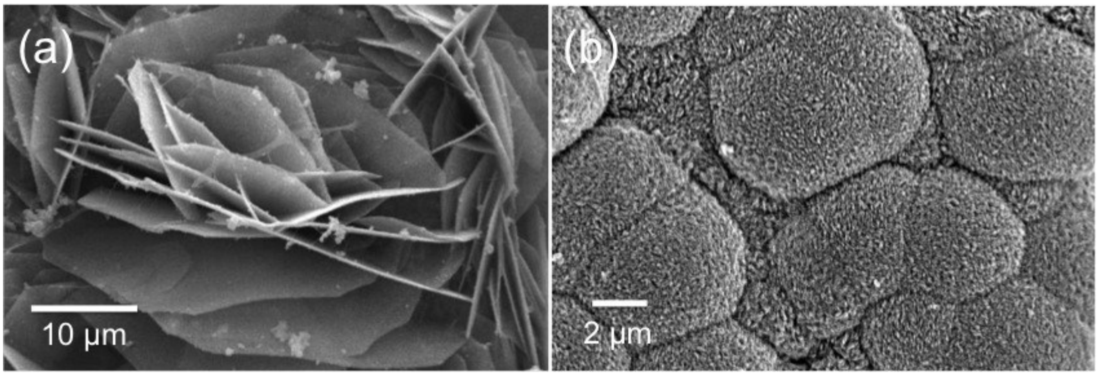

Figure S3: SEM images of (a) Co_3O_4 nanoflakes and (b) CuO nanostructures on Ni foam.

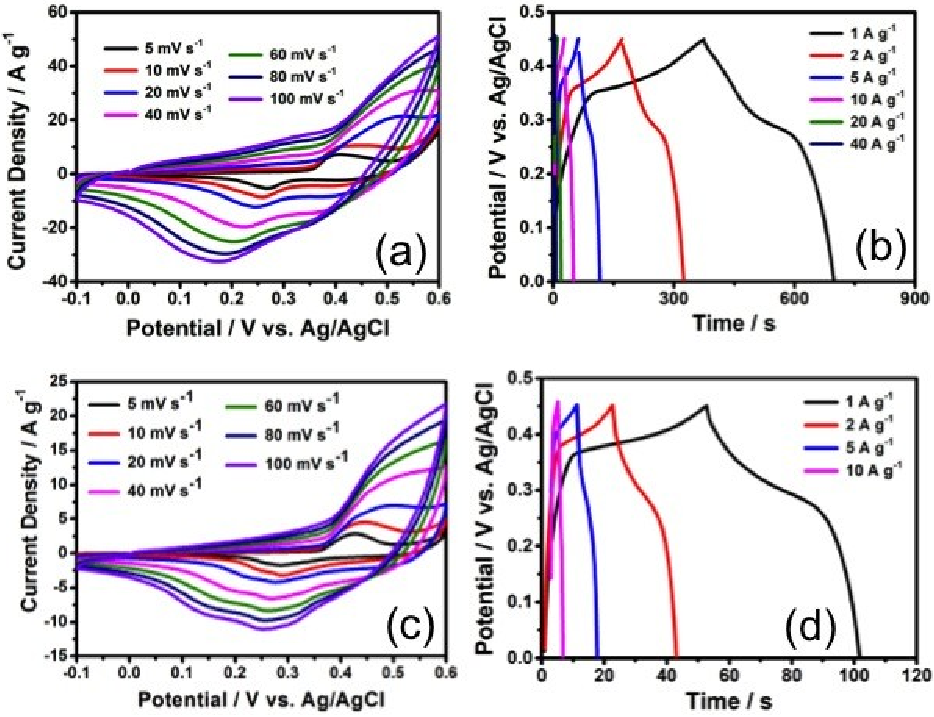

Figure S4: (a, c) CV diagrams and (b, d) GCD profiles of Co_3O_4 nanoflakes (a, b) and CuO nanostructures (c, d) in a three-electrode system.

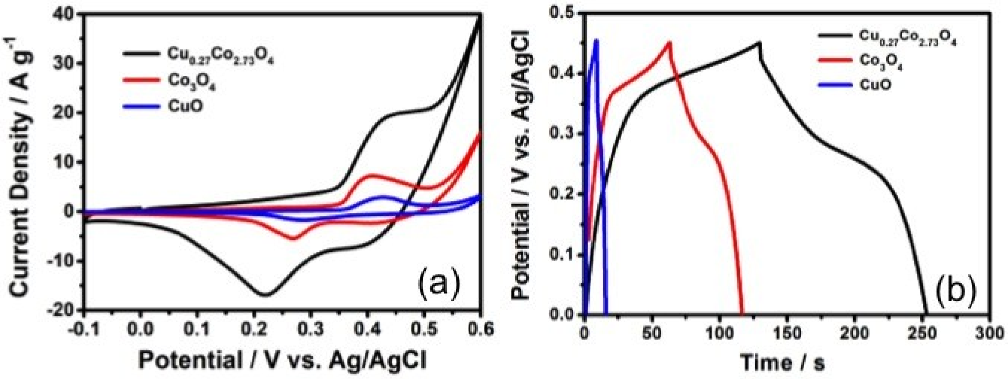

Figure S5: Comparison of (a) CV diagram at 5 mV s^{-1} scan rate and (b) GCD profile at 5 A g^{-1} current density for $Cu_{0.27}Co_{2.73}O_4$, Co_3O_4 and CuO.

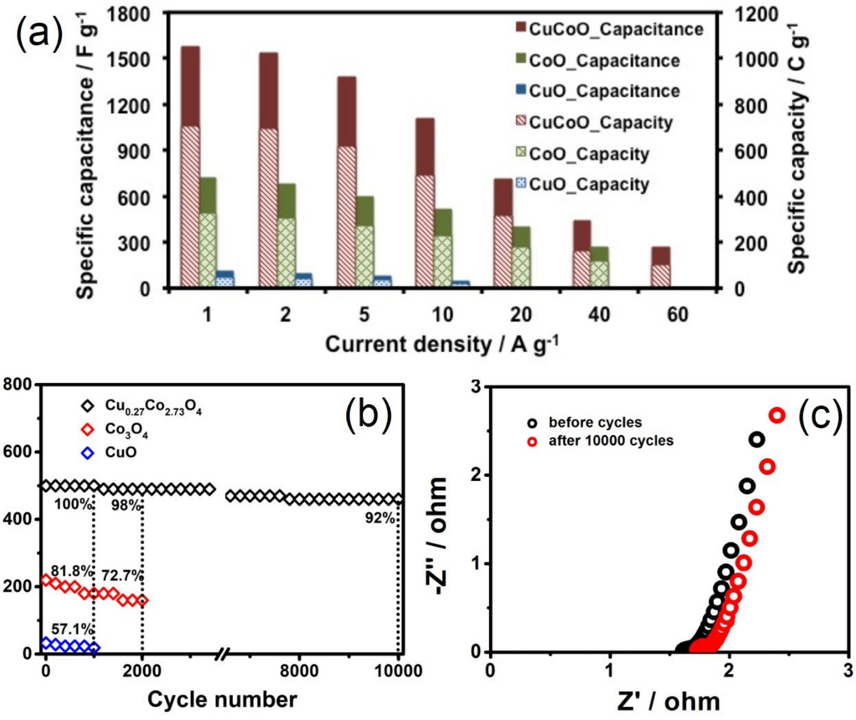

Figure S6: Supercapattery performances in a three-electrode system: (a) Variation of specific capacitance and specific capacity obtained at different current densities for samples; (b) cyclic performance of $Cu_{0.27}Co_{2.73}O_4$ (10 A g^{-1}/10,000 cycles), Co_3O_4 (10 A g^{-1}/2000 cycles) and CuO (2 A g^{-1}/1000 cycles); (c) Nyquist plot for $Cu_{0.27}Co_{2.73}O_4$ electrode before and after 10,000 cycles (10 A g^{-1}).

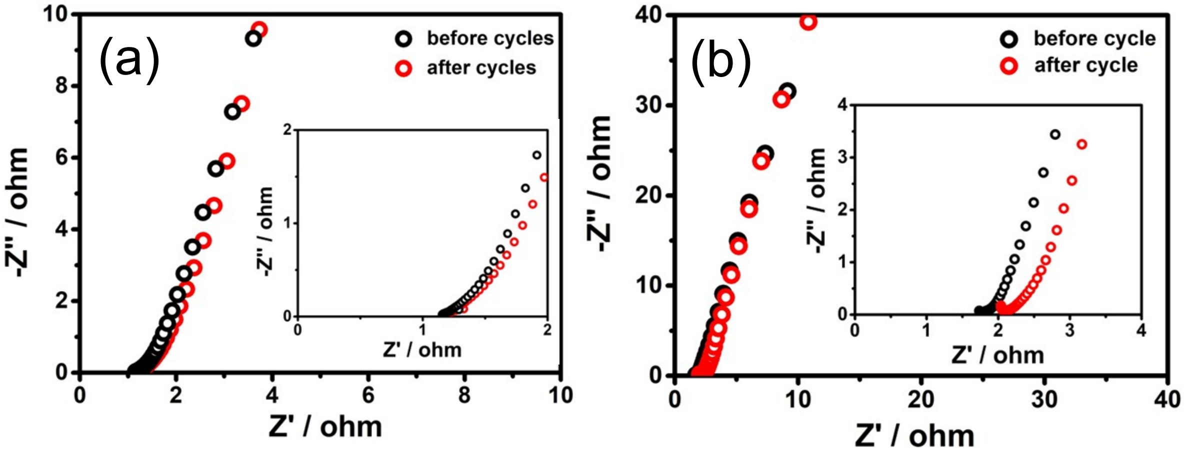

Figure S7: Nyquist plots of (a) Co_3O_4 and (b) CuO before and after stability test.

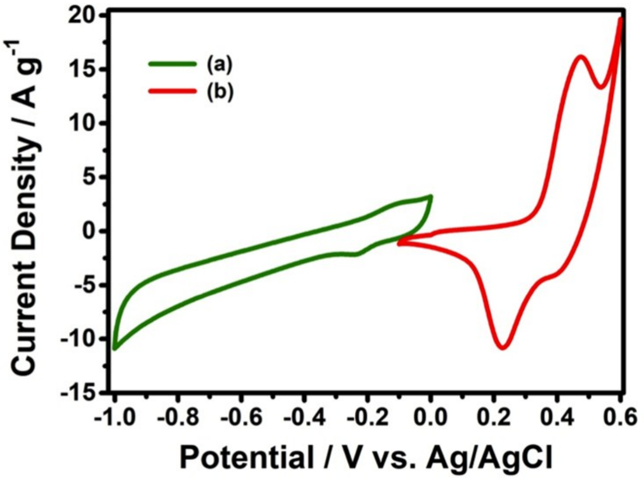

Figure S8: CV diagrams of charge-balanced $Cu_{0.27}Co_{2.73}O_4$ and AC electrodes at a scan rate of 5 mV s^{-1} in a three-electrode system.

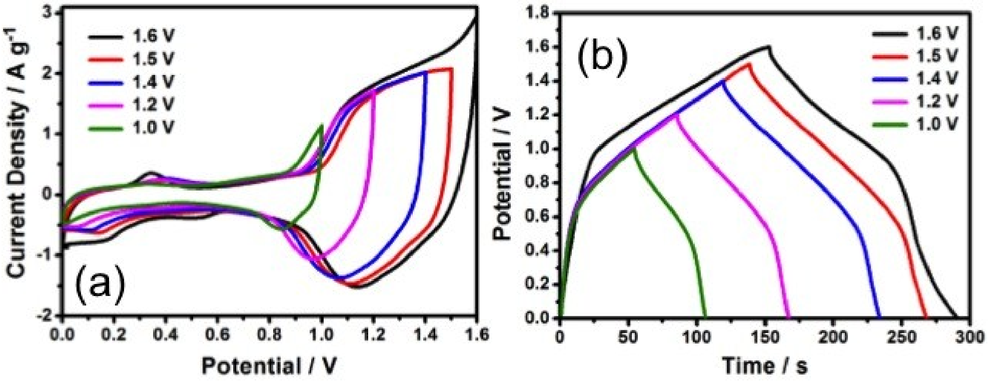

Figure S9: (a) CVs at 10 mV s^{-1} and (b) GCDs at 1 A g^{-1} of CCO//AC at different potential windows.

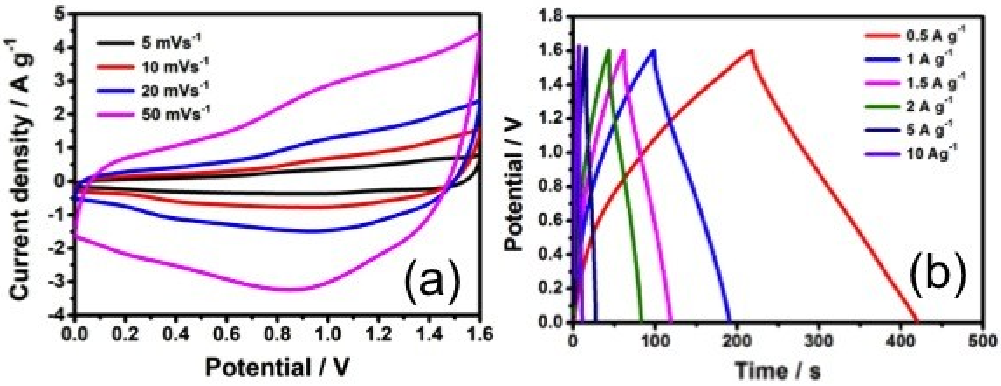

Figure S10: (a) CV diagram at different scan rates and (b) GCD profile at different current densities of CO//AC device in a potential window 0 – 1.6 V.

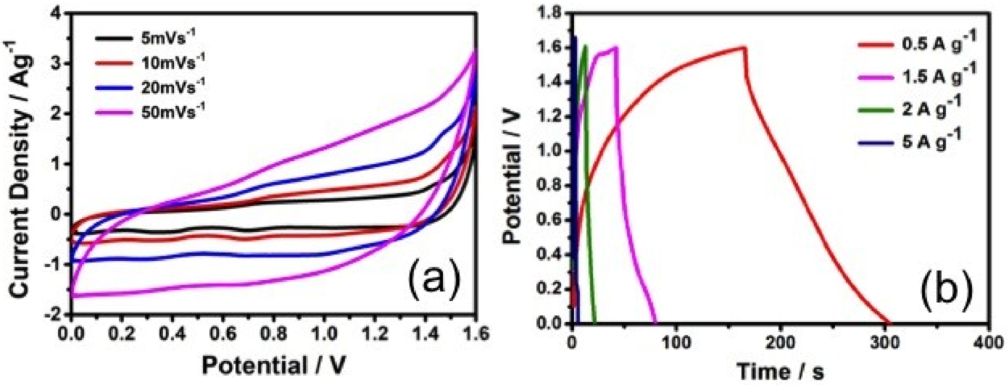

Figure S11: (a) CV diagram at different scan rates and (b) GCD profile at different current densities of CuO//AC device in a potential window 0 – 1.6 V.

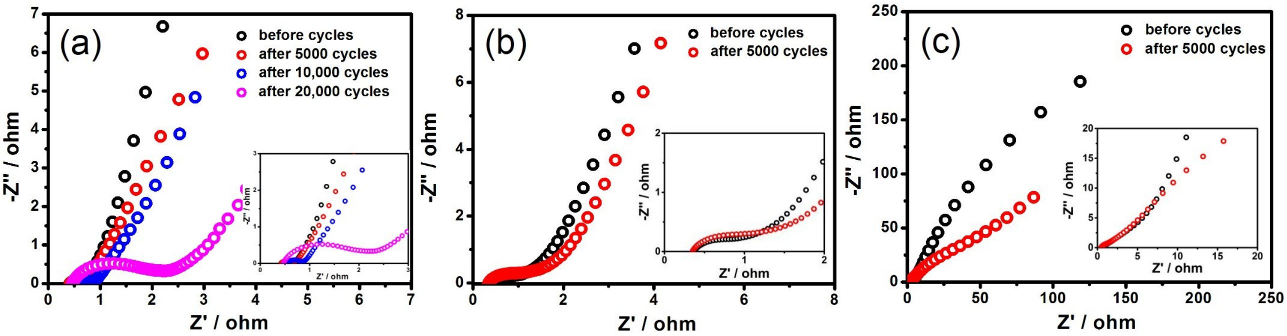

Figure S12: Nyquist plot of before and after cyclability test for (a) CCO//AC, (b) CO//AC, and (c) CuO//AC.

Table S1: EIS analyses of CCO//AC, CO//AC and CuO//AC asymmetric devices at different cycles.

Cycles	CCO//AC		CO//AC		CuO//AC	
	R_s (ohm)	R_{ct} (ohm)	R_s (ohm)	R_{ct} (ohm)	R_s (ohm)	R_{ct} (ohm)
0	0.42	0.25	0.35	0.85	0.47	5.65
5000	0.43	0.26	0.35	1.25	0.47	41.57
10000	0.52	0.31	--	--	--	--
20000	0.48	1.77	--	--	--	--

Table S2: Comparison of the Performance of copper cobaltite and cobalt compound-based asymmetric supercapacitors systems in literatures.

Asymmetric system		Sp. capacity/ capacitance @ current density	Energy density (Wh kg^{-1})	Power density (W kg^{-1})	Cycle number	Capacity retention	Ref.
Copper cobaltite based electrodes*	$CuCo_2O_4$ double- shelled hollow spheres//AC	119.4 F g^{-1} @ 20 mA cm^{-2}	37.3	1500	6000	92.5%	3
	$CuCo_2O_4$//AC	137 F g^{-1} at 1 A g^{-1}	42.81	750	6000	86%	4
	$CuCo_2O_4$/CuO//RGO/ Fe_2O_3	83 F g^{-1} @ 0.5 A g^{-1}	33	200	5000	88%	5
	$CuCo_2O_4$@$CuCo_2O_4$//AC	57.60 F g^{-1} @ 2 mA cm^{-2}	18	125	2000	101%	6
	Electrospun $CuCo_2O_4$ NW//AC	183 mF cm^{-2} @ 15 mA cm^{-2}	0.81 mWh cm^{-3}	7.48 mW cm^{-3}	3000	82%	7
	Flower-like $Cu_{0.27}Co_{2.73}O_4$//AC	161.04 C g^{-1} (100.65 F g^{-1}) @ 0.5 A g^{-1}	35.78	400	@ 5 A g^{-1}		This work
					20,000	86.9%	
					10,000	91.3%	
					@ 10 A g^{-1}		
					10,000	95%	
Other cobalt-based promising electrodes	Ni,Co-Hydroxyl Carbonate//Hierarchical porous carbon (all-solid state ASCs)	130 F g^{-1} @ 0.5 A g^{-1}	30	8.69	19,000 (@ 2 A g^{-1})	100% (Solid state ASC)	8
	Nickel cobalt ammonium phosphate@ nickel cobalt ammonium phosphate// Hierarchical porous carbon	105 F g^{-1} @ 0.5 A g^{-1}	44.5	7.4	7000	77.5%	9
	Nickel Cobalt Hydroxide @Reduced Graphene Oxide// Hierarchical porous carbon	150 F g^{-1} @ 0.5 A g^{-1}	56.1	76	17000	80%	10
	NiCoP nanosheets//AC	100 F g^{-1} @ 1 A g^{-1}	43.54	150	8000	90.6%	11

*Copper cobaltite based electrode performance other than two-electrode asymmetric system has not been compared.

1. R. Li, Z. Lin, X. Ba, Y. Li, R. Ding and J. Liu, *Nanoscale Horizon*, 2016, **1**, 150-155.
2. S. Sun, S. Wang, S. Li, Y. Li, Y. Zhang, J. Chen, Z. Zhang, S. Fang and P. Wang, *J Mater. Chem. A*, 2016, **4**, 18646-18653.
3. S. Kamari Kaverlavani, S. E. Moosavifard and A. Bakouei, *Chemical communications*, 2017, **53**, 1052-1055.
4. A. Pendashteh, S. E. Moosavifard, M. S. Rahmanifar, Y. Wang, M. F. El-Kady, R. B. Kaner and M. F. Mousavi, *Chem. Mater.*, 2015, **27**, 3919-3926.
5. Y. Wang, C. Shen, L. Niu, R. Li, H. Guo, Y. Shi, C. Li, X. Liu and Y. Gong, *J Mater Chem A*, 2016, **4**, 9977.
6. Y. Zhang, J. Xu, Y. Zheng, Y. Zhang, X. Hu and T. Xu, *RSC Adv*, 2017, **7**, 3983-3991.
7. Q. Wang, D. Chen and D. Zhang, *RSC Adv*, 2015, **5**, 96448–96454.

8. Y. Zhao, H. Ma, S. Huang, X. Zhang, M. Xia, Y. Tang and Z. F. Ma, *ACS Appl Mater Interfaces*, 2016, **8**, 22997-23005.
9. M. Wang, Y. Zhao, X. Zhang, R. Qi, S. Shi, Z. Li, Q. Wang and Y. Zhao, *Electrochim Acta*, 2018, **272**, 184-191.
10. H. Ma, J. He, D. B. Xiong, J. Wu, Q. Li, V. Dravid and Y. Zhao, *ACS Appl Mater Interfaces*, 2016, **8**, 1992-2000.
11. X. Zhang, A. Wu, X. Wang, C. Tian, R. An and H. Fu, *J Mater. Chem. A*, 2018, DOI: 10.1039/C1038TA05551C.